JOURNAL OF GUIDANCE, CONTROL, AND DYNAMICS
Vol. 19, No. 2, March–April 1996

Improved Tunnel Display for Curved Trajectory Following: Control Considerations

Arthur J. Grunwald*
Technion—Israel Institute of Technology, Haifa 32000, Israel

Improvements of a previously developed tunnel display for curved trajectory following are presented and theoretically analyzed. The success of earlier versions of this display can be attributed to the combination of the perspective tunnel image with a superimposed predictor symbol. The tunnel image provides the spatial awareness and preview of the trajectory forcing function, and the predictor provides vital guidance and control information. Two main shortcomings of these earlier versions, occurring for large and sluggish aircraft requiring longer prediction times, are addressed: 1) poor performance in transitions between straight and curved trajectory sections and 2) poor positional accuracy in the presence of biases or low-frequency disturbances. The two basic improvements addressing these shortcomings, and incorporated into an improved display layout, are 1) an algorithm for generating trajectory shapes that are well matched with the average vehicle response and 2) an actively driven predictor reference window, yielding improved predictor guidance information. The improvements combine the advantage of a vehicle path predictor that performs as a well-designed natural flight director, with improved curve transition behavior and improved positional accuracy in the presence of slowly varying cross winds.

Introduction

PICTORIAL perspective displays, like the tunnel or pathway-in-the-sky display, are commonly recognized as meaningful candidates for a primary integrated flight display. Among others, the choice of these types of display is motivated by the requirement for following complex and curved trajectories,[1] a need for enhancing spatial awareness,[2–4] a way of presenting the flight information in a natural and integrated format,[5–8] or the need for the tunnel as a conformal three-dimensional path overlay in enhanced/synthetic vision systems.[9]

Furthermore, complex and rapidly changing air traffic control environments, e.g., as managed by the proposed Center-Tracon Automation System (CTAS)[10] under development, require the ability to adjust and modify four-dimensional trajectories on-line and require these trajectories to be custom tailored to a specific aircraft response. The ease by which the tunnel display allows the pilot to handle these unexpected vehicle-specific trajectory modifications, in particular, makes this kind of display suitable for these dynamic environments.

The advent of a differential global positioning system that makes accurate three-dimensional position information available onboard, together with rapid developments in affordable onboard computers and high-resolution color graphics displays, has brought the practical implementation of the tunnel display well within reach. Furthermore, new aeronautics programs, such as the High-Speed Civil Transport, which employs synthetic vision for the approach to landing and advanced subsonic technology that includes the tilt rotor with its transition from forward to vertical flight, offer potential applications of the concept. The renewed interest in the tunnel display has motivated us to address shortcomings encountered in versions developed in earlier work.[11–13] Although this type of display performed very well in straight, as well as steady curved, trajectory sections, path-following accuracy in transitions between straight and curved trajectory sections and in the presence of strong cross winds was degraded under certain conditions. Although increased pilot skill and familiarization with one particular trajectory or situation[1] can compensate for these shortcomings, this paper presents a systematic and general solution for this problem.

The display layout of the tunnel display version developed previously[11,12] is shown in Fig. 1a, and the corresponding horizontal situation is shown in Fig. 1b. The attributes of this display are 1) the perspective tunnel image, which represents an inside-out view of the winding and descending desired spatial trajectory, 2) the predictor, which is a point on the circular future vehicle path and which is moving along with the vehicle at a given prediction time ahead, 3) the tunnel cross section square, which is moving along at the same prediction time ahead, 4) velocity control tick marks used for flying a velocity profile in four-dimensional approaches, and 5) the horizon bar providing the pitch and roll attitude reference. The success of this earlier tunnel display version is attributed to the useful combination of the perspective tunnel image with the overlaid predictor symbol. The tunnel image provides the situational awareness and preview of the trajectory forcing function, and the predictor symbol provides the guidance and control information. It is shown in Ref. 12 that the predictor, being a point on the circular predicted vehicle path with radius R_p and tangential to the velocity vector V as shown in Fig. 1b, furnishes the transfer function of the effectively controlled element, i.e., the transfer between a lateral stick command and a lateral displacement, with an optimally damped second-order lead term of the form

$$H_p(s) = \tfrac{1}{2}T_p^2 s^2 + T_p s + 1 \tag{1}$$

where T_p is the prediction time and s the Laplace operator. An additional advantage of the circular path predictor is that, in the absence of disturbances, it enables a zero steady-state error in flying constantly curved trajectory sections. Thus, the predictor both furnishes the system with the necessary damping cues and assists the pilot in coping with the trajectory curvature forcing function by providing the correct control command information. The combination of tunnel and predictor symbol allows both a very smooth trajectory-following performance and a fast, smooth and well-damped capture of the trajectory from a random location outside the tunnel.[11,12] In addition to providing damping cues and command information, the predictive information is also used in controlling the forward velocity of the aircraft in four-dimensional approaches.[12] This is accomplished by using the changes in predictor distance as a control cue. These changes result from the changes in velocity and longitudinal acceleration and are visualized by the displacement of the tick marks from the tunnel square. The forward velocity is controlled by adjusting the position of the tick marks along the trajectory by means of the throttle. By using a suitable display law,[12] a smooth and well-damped throttle response to a desired velocity change can be obtained. Although this method of controlling the forward velocity was found to be very effective in four-dimensional fixed-wing

Received Nov. 17, 1993; revision received June 30, 1995; accepted for publication Oct. 5, 1995.

*Associate Professor, Faculty of Aerospace Engineering. Member AIAA.

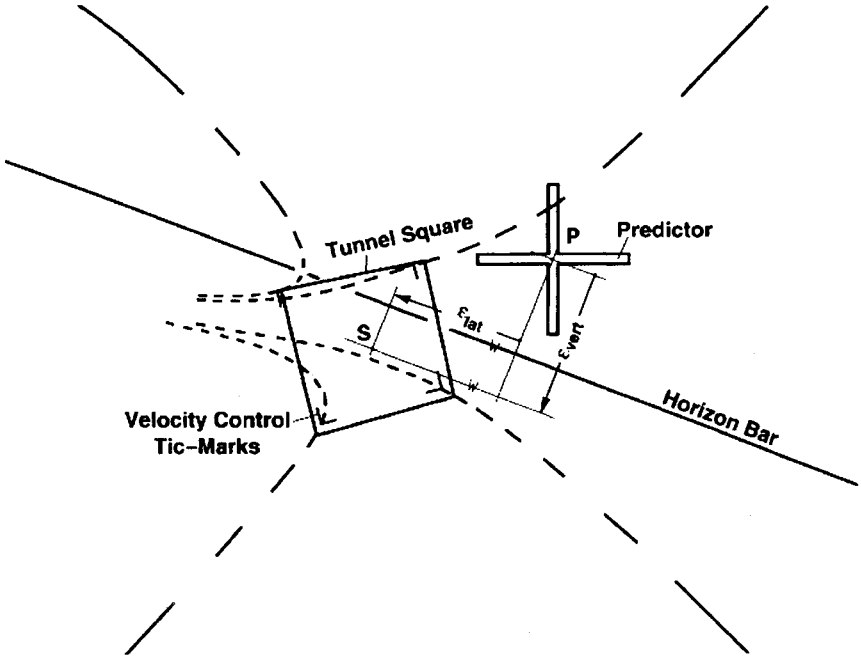

Fig. 1a Display layout of the original tunnel display.

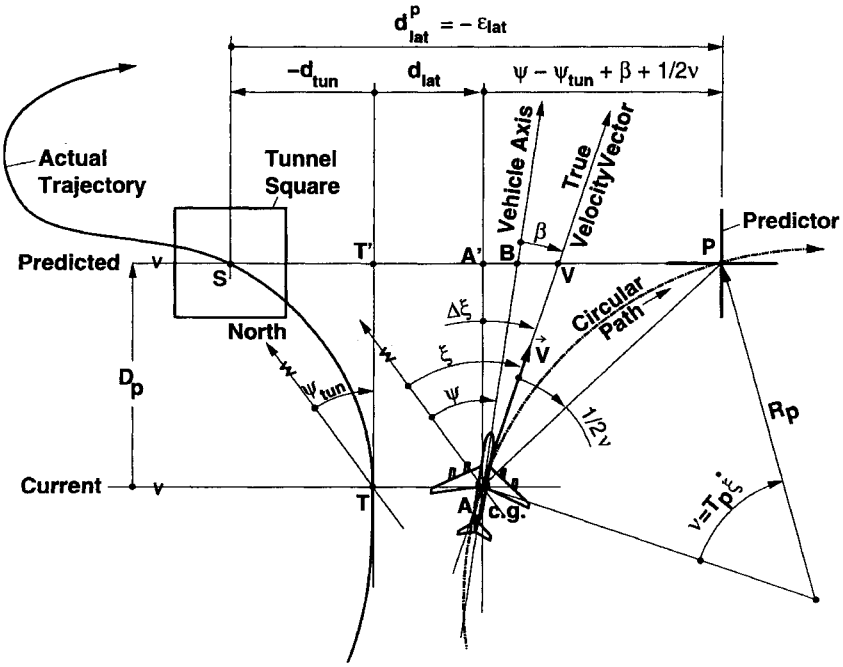

Fig. 1b Horizontal situation of the original tunnel display.

aircraft approaches, the use of a predictor to combine forward, vertical, and lateral velocity information in one display format is expected to be useful in particular for nonconventional aircraft that operate on both the front and backside of the power curve, such as the Harrier or the tilt rotorcraft. By blending predictive information with well-designed guidance information, the display is expected to assist the pilot in smoothly and accurately transitioning from forward flight to hovering flight.

Although, in curved approaches, the tunnel display has clear advantages over more conventional flight-director displays, large and sluggish aircraft for which larger prediction times are used exhibit a less accurate lateral tunnel-following performance in transitions between straight and curved trajectory sections. Since the trajectory is normally composed of straight sections and curved sections with a constant radius, the trajectory curvature function is discontinuous. In most cases the degraded path-following accuracy can be attributed to corner cutting, resulting from banking the aircraft before its actual entry into the curve (for transitions from straight to curved sections) and leveling the aircraft before its entry into a straight section (for transitions from curved to straight sections). It is clear that these larger aircraft have distinct difficulties in following trajectories with discontinuities in the curvature function and that gradual transitions between straight and curved sections that would match the vehicle response are essential. In fact, the online computation of aircraft-specific trajectories is a necessity in the automated management and control of terminal area traffic, such as CTAS,[10] in which global minimization of fuel cost and delays is sought.

A second shortcoming resulting from the large prediction times required for large and sluggish aircraft is the deterioration of path-following accuracy in the presence of biases or slowly varying disturbances. The sensitivity to these biases is apparent from Eq. (1), which shows that an increase in prediction time T_p results in an

increase in the velocity and acceleration gain, whereas the position gain remains unchanged.

For large and sluggish aircraft, tunnel-following behavior in transition sections can be greatly improved by using a continuous trajectory curvature function that best matches with the average natural vehicle response. For this purpose, a relatively simple trajectory generation algorithm has been developed that uses the trajectory waypoints, the velocity, and the stability derivatives of the basic roll rate response of the aircraft as input data. The sensitivity to biases and slowly varying disturbances can be greatly reduced by providing improved predictor guidance information embedded in an improved display layout. Both developments require relatively small increases in the original onboard computational requirements and are discussed hereafter.

Trajectory Generation Algorithm

Evaluations of the original tunnel display have shown that a tunnel trajectory, composed of straight and curved sections with a constant radius, can be flown quite smoothly by bringing the predicted lateral and vertical deviation, i.e., the deviation between predictor cross and tunnel square, to zero, provided the predictor distance D_p is chosen sufficiently large for the given vehicle dynamics; see Fig. 1b. This notion is now used to create a tunnel trajectory that best matches with the average vehicle response. The trajectory generation algorithm operates in four stages. First, the three-dimensional trajectory waypoints are defined; in actual flight, for instance, these points could be obtained either by retrieving them from a disk file of instrument flight rule map data or by receiving them online from an air traffic control center. Second, the waypoints are interconnected by straight trajectory sections. At the vertices of the trajectory, curved sections with a constant radius are introduced, tangential to the straight sections. The radius of turn of the curved sections is chosen such that, for the given velocity, a maximum allowed bank angle is not exceeded. Third, this raw trajectory is flown by a paper aircraft and paper pilot in a fast-time simulation run, using the deviation of the predictor cross from the tunnel square as the control error. The inertial position of the aircraft and the aircraft yaw, pitch, and roll attitude angles are recorded at discrete points of the trajectory, here 200 ft of traveled distance apart. Fourth, the three-dimensional tunnel structure is generated by centering a rectangular tunnel element at each one of the trajectory points and by orienting the element such that it is perpendicular to the vehicle path, with its base parallel to the vehicle wing line. The corners of the rectangles form the outline of the tunnel structure. Thus, the tunnel elements are banked in curves, where the bank angle matches the one required for carrying out a coordinated turn at the given velocity.

A block diagram of the linearized lateral control system used in the fast-time simulations is shown in Fig. 2. Following Fig. 1b, the predicted lateral deviation d_{lat}^p is composed of the following terms:

$$d_{\text{lat}}^p = d_{\text{lat}} + \left(\psi - \psi_{\text{tun}} + \beta + \tfrac{1}{2}\nu\right) D_p - d_{\text{tun}} \tag{2}$$

where d_{lat} is the actual lateral deviation from the trajectory; ψ is the actual vehicle heading and ψ_{tun} the tunnel heading, both with respect to the magnetic north; β is the crabbing angle between the vehicle axis and the ground-referenced velocity vector V; also, ν is the arc length of the prediction span, D_p the predictor distance, and d_{tun} the portion of the predicted lateral deviation because of the curvature of the tunnel. In this linear analysis, the angles $\psi - \psi_{\text{tun}}$, β, and ν are assumed to be relatively small. For the right-hand system shown in Fig. 1b with the yaw axis pointing away from the viewer, a left tunnel trajectory curve corresponds to a negative curvature and yields a negative value of d_{tun}. A deviation in the negative direction is indicated in Fig. 1b with a minus sign. Equation (2) is implemented in block diagram form in Fig. 2. Since the circular path predictor assumes a constant path-angle turn rate over the prediction span, it follows that

$$\nu = T_p \dot{\xi} \tag{3}$$

Furthermore, the angle of deviation $\Delta\xi$ of the velocity vector from the direction of the trajectory, $\Delta\xi = \psi - \psi_{\text{tun}} + \beta$, determines the rate of deviation from the trajectory according to

$$\Delta\xi = \dot{d}_{\text{lat}} / V \tag{4}$$

where V is the ground speed. Substituting Eqs. (3) and (4) into Eq. (2) and using the fact that $T_p = D_p / V$ yields

$$d_{\text{lat}}^p = \tfrac{1}{2} T_p^2 \ddot{d}_{\text{lat}} + T_p \dot{d}_{\text{lat}} + d_{\text{lat}} - d_{\text{tun}} \tag{5}$$

Thus, d_{lat}^p includes the position, the rate, and the acceleration of the actual lateral deviation that results in the second-order lead term of Eq. (1). As shown in Fig. 2, the predicted lateral deviation is compared with the null reference to obtain the control error $\varepsilon_{\text{lat}} = -d_{\text{lat}}^p$, which is used in a simple proportional control law to create the command $p_{\text{com}} = K_\varepsilon^{\text{lat}} \varepsilon_{\text{lat}}$ to the roll-rate command system. This system consists of a simplified first-order representation of the vehicle roll-rate response, an aileron servo, and a proportional roll-rate control loop closure $\delta_a = K_p(p_{\text{com}} - p)$. It has been shown[14] that a vehicle with a well-designed lateral augmentation system, i.e., with adequately damped Dutch roll mode and correct turn coordination, can be approximated by its first-order roll subsidence mode. The dimensional stability derivatives L_p and $L_{\delta a}$ characterize the lateral vehicle dynamics. The shape of the tunnel trajectory is determined by the guidance gain $K_\varepsilon^{\text{lat}}$, the roll autopilot gain K_p, and the prediction time T_p. These values should be chosen such that entries to and from curved sections are as fast as possible, with minimum deviation from the raw trajectory and without overshoot.

In this example the velocity is $V = 220$ ft/s, $L_{\delta a} = 2.0\ \text{s}^{-2}$, $L_p = -1.0\ \text{s}^{-1}$, and $K_p = 1.0$ s. A suitable value for $K_\varepsilon^{\text{lat}}$ is 0.0025 for $T_p = 6$ s. Time histories of the fast-time simulations with an exemplary trajectory with four straight and three curved sections, for $T_p = 6$ s, are shown in Fig. 3. The stepwise character of the curvature function of the raw trajectory is smoothed by the algorithm, which manifests itself in transition sections with gradually

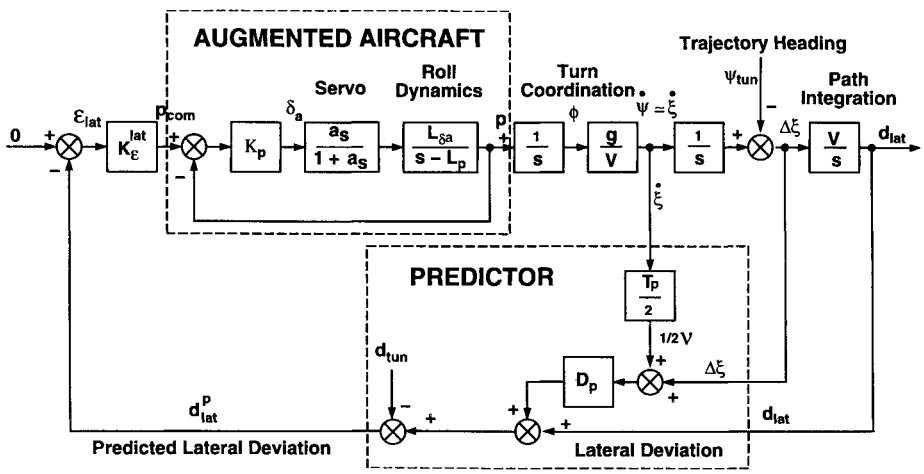

Fig. 2 Block diagram of fast-time simulation of lateral control.

increasing and decreasing curvature. For ease of interpretation, the curvature is expressed in terms of an equivalent bank angle ϕ. For a coordinated turn, the curvature is $1/R_t = (g/V^2)\tan\phi$, where g is the gravity acceleration. Figure 3 also shows the deviation from the raw trajectory. The transition sections for the smoothed trajectory, however, reduce the length of the sections with constant curvature. Since the flying of a section with a constant curvature has the advantage that the vehicle can settle into a steady-state condition with fixed bank angle and zero predicted and actual lateral deviations, the smoothed trajectory with its reduced constant curvature sections will require somewhat more control activity from the pilot. Therefore, the smoothed trajectory should have the shortest transition sections that still result in acceptable roll rates and deviations from the raw trajectory.

Improved Display Layout

As mentioned earlier, in the original tunnel display the predictor cross represented the predicted future vehicle position and the tunnel cross-section square the desired future position. A control strategy aimed at keeping the cross centered on the square would therefore bring the predicted lateral and vertical deviations to zero. If the prediction was indeed correct, the actual deviations would eventually go to zero as well. To allow the cross to be accurately placed on the square, the cross and square were of the same outer dimensions (Fig. 1a). Note that the lateral and vertical deviations

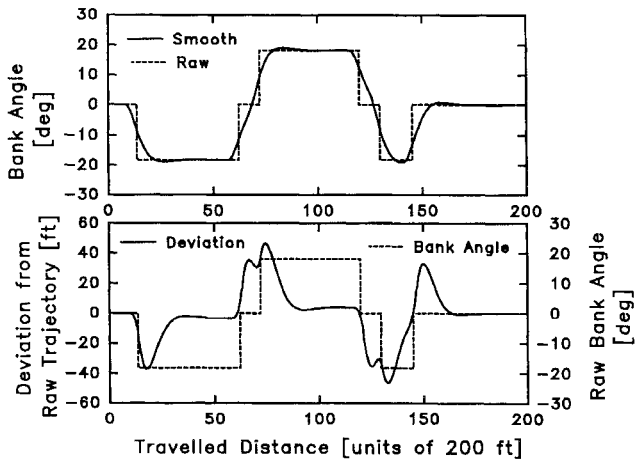

Fig. 3 Time histories of fast-time simulation of lateral control.

ε_{lat} and ε_{vert} are measured in directions parallel and perpendicular to the horizon, respectively.

The improved tunnel display layout is shown in Fig. 4a and the corresponding horizontal situation in Fig. 4b. Two tunnel cross sections are drawn, both moving along with the aircraft at constant prediction times ahead. The tunnel has a constant square cross section of dimensions 300 × 300 ft. The nearer square is 2 s ahead and the farther square 6 s ahead. The square at $T_p = 2$ s accommodates the lateral and vertical deviation indicators. These indicators display the actual (zero prediction time) displacements at a scale enlarged by a factor of 2.5. Thus, when the indicators are at the right top corner of the square, the aircraft is 60 ft to the right and 60 ft above the desired trajectory. The need for the explicit display of outside-in displacement information has been expressed in pilot comments recorded during earlier experimental evaluation of the tunnel display.[13] By attaching the indicators to the square 2 s ahead, the displacement information is integrated in a natural way into the perspective image without cluttering or obscuring the central area of the display.

The square at 6 s ahead accommodates the predictor guidance information. In contrast to the original tunnel display, the predictor symbol is reduced to one-quarter of the size of the tunnel square, i.e., 75 ft in width. The cross-section square, which in the original tunnel display was drawn as an outline only, now appears as a half-transparent plane with a guidance cutout window, the size of the predictor. The cutout window can be moved with respect to the center of the square. Its displacements are driven by the guidance logic in a fashion that assures significantly improved trajectory following if the pilot simply acts to drive the predictor symbol into the cutout window. In effect, by driving the cutout window rather than the tunnel square, we have transformed the earlier error regulation task into a command tracking task. The specific format of a half-transparent square with cutout window has been chosen to assure that the cutout window appears in the plane of the tunnel square. This would not be the case if both the square and the cutout window were to be drawn as outlines, since the cutout window with its smaller apparent size, would appear to be at a farther distance, because of perspective cueing.

Figure 4a also shows that from the tunnel structure only the tunnel corner lines are drawn. Alternately, the corners of two successive tunnel elements 200 ft apart are interconnected, which results in the dashed pattern. The advantage of this structure is that the spatial trajectory is outlined with a minimum of lines, whereas the visual flow of the 200-ft-length line segments provides the impression of forward motion.

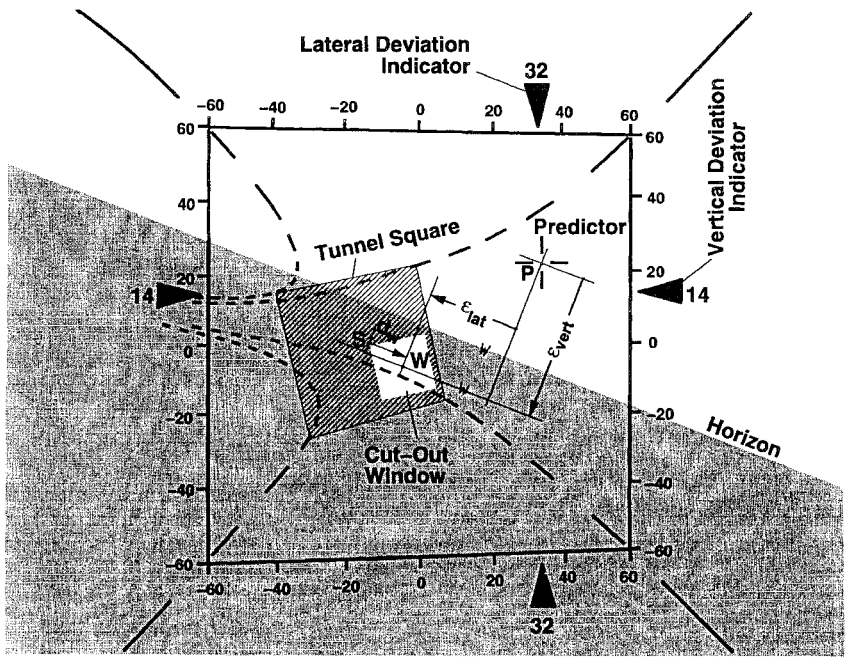

Fig. 4a Display layout of the improved tunnel display.

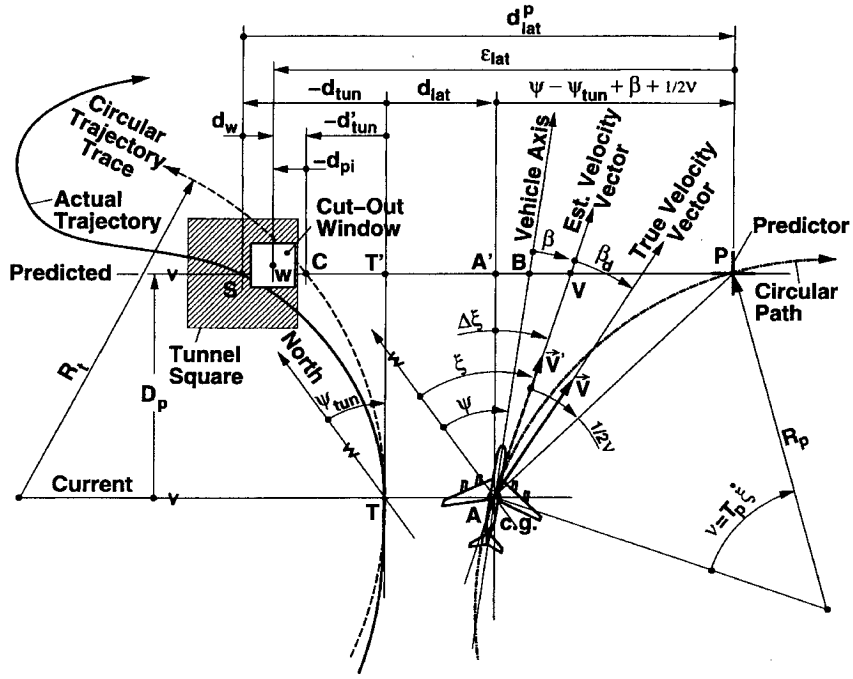

Fig. 4b Horizontal situation of the improved tunnel display.

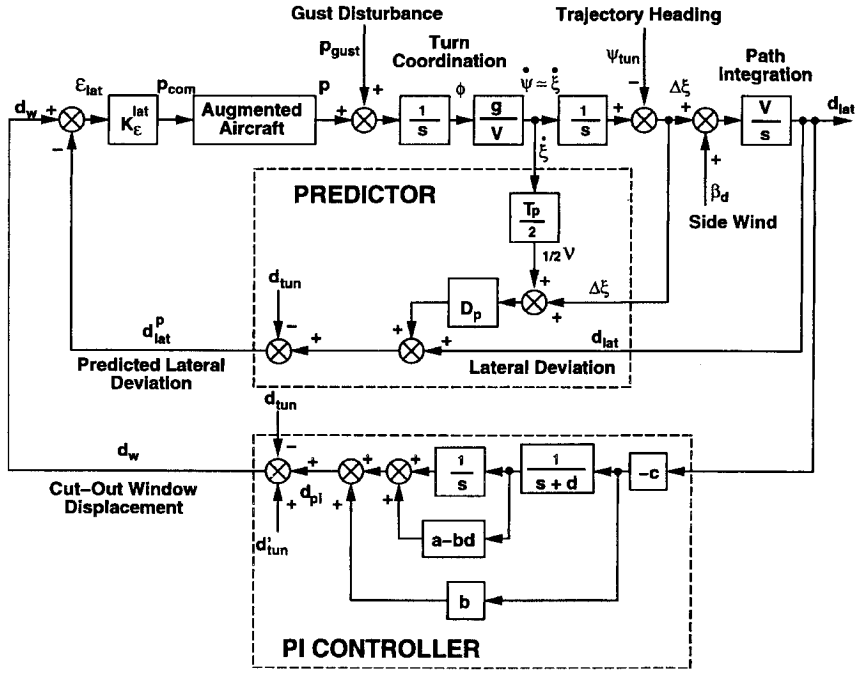

Fig. 5 Block diagram of the cutout guidance window operation.

Predictor Guidance Information

Figure 4b shows the use of the cutout window for providing improved predictor guidance information. Two improvements are made. The first one reduces the corner cutting as it appeared in transition sections with the original tunnel display. Correct trajectory following would require that, at all times, the trajectory curvature matches the vehicle path curvature. For the original circular path predictor, this is the case only in straight or constantly curved sections. In transition sections, the predictor displacement from the tunnel square encourages the pilot to bank the vehicle before the change in trajectory curvature has actually taken place. This premature banking results in considerable corner cutting, especially for larger prediction times.

To correct for corner cutting, we can modify the guidance scheme to require that the predictor cross (point P) be kept on the circular dotted trajectory trace (point C), rather than on the actual trajectory (point S), as shown in Fig. 4b. This trace is tangential to the trajectory at the location T, with a radius R_t that corresponds to the trajectory curvature at that location. In transitions from straight to curved sections, by appropriate lateral motion of the cutout window, the onset of the banking cue will be delayed until the aircraft has actually reached the curved section. In sections with a constant curvature, however, the cutout window will remain centered at the tunnel square, and the situation will be identical to that of the original tunnel display. This arrangement markedly reduces corner cutting.

A second improvement addresses the effect of biases and/or low-frequency disturbances. Since the circular predictor path is ground referenced, it requires accurate measurement of the ground speed vector. In the presence of steady cross winds, large biases in the estimate of the ground speed vector might occur if this vector is derived from a directional gyro and an onboard sideslip sensor that measures the sideslip with respect to the air mass rather than the ground. This situation is represented in Fig. 4b, where the predictor trace is based on the biased velocity vector V' instead of the true

vector V. The directional error in V is represented by the angle β_d. For the larger prediction times, the error in the estimate of the ground speed vector will result in excessively large actual lateral deviations. This shortcoming is greatly overcome by providing a certain degree of integral control action to the guidance cutout window.

The block diagram in Fig. 5 shows how both improvements are realized. The augmented aircraft represents the vehicle with the roll-rate command system, illustrated earlier in Fig. 2. The augmented aircraft, vehicle path kinematics, and the predictor block are the same as well. Added to the diagram are a roll-rate gust disturbance p_{gust}, a side-wind disturbance β_d, and a second-order proportional-integral (PI) controller composed of a first-order lag and an integrator. The integral action is realized by passing the measured actual lateral deviation d_{lat} through this controller and generating an output d_{pi}, given by

$$d_{pi}(s) = -\frac{c(bs^2 + as + 1)}{s(s + d)} d_{\text{lat}}(s) \tag{6}$$

where a, b, c, and d are the controller constants. The cutout window W is displaced in the horizontal direction (parallel to the horizon) with respect to the center of the tunnel square S by the amount d_w given by (see Fig. 4b)

$$d_w = d_{pi} + d'_{\text{tun}} - d_{\text{tun}} \tag{7}$$

where d_{tun} is the portion of the predicted lateral deviation because of the actual trajectory shape and d'_{tun} is the portion referenced to the circular dotted trajectory trace. The displacement d_w constitutes the command input to the control system. The lateral deviation of the predictor symbol from the cutout window constitutes the control error that the pilot attempts to minimize. This control error is given by

$$\varepsilon_{\text{lat}} = d_w - d^p_{\text{lat}} = d_{pi} + d'_{\text{tun}} - d_{\text{tun}} - d^p_{\text{lat}} \tag{8}$$

Substituting d_{pi} of Eq. (6) and the Laplace transformed expression for d^p_{lat} of Eq. (5) into Eq. (8) yields

$$\varepsilon_{\text{lat}}(s) = -\left[\frac{c(bs^2 + as + 1)}{s(s + d)} + \left(\frac{1}{2}T_p^2 s^2 + T_p s + 1\right)\right] \times d_{\text{lat}}(s) + d'_{\text{tun}}(s) \tag{9}$$

Equation (9) constitutes the loop-closure dynamics of the atmospheric-disturbance free control system. By choosing $a = T_p$ and $b = 0.5T_p^2$, Eq. (9) simplifies to

$$\varepsilon_{\text{lat}}(s) = -\frac{\left(\frac{1}{2}T_p^2 s^2 + T_p s + 1\right)(s^2 + ds + c)}{s(s + d)} d_{\text{lat}}(s) + d'_{\text{tun}}(s) \tag{10}$$

where Eq. (10) shows that the loop-closure dynamics includes both the vital optimally damped lead zeros of Eq. (1) and the integral control action. The values of the constants c and d should be chosen such that the zeros of the second lead term in Eq. (10) are distinct, with one lead zero close to the origin. The amount of integral action is determined by the distance of this zero from the origin. Root locus plots of the closed-loop system poles near the origin, as a function of the pilot gain $K^{\text{lat}}_{\varepsilon}$, for prediction times of 3, 6, and 9 s are shown in Fig. 6. It is shown that for a sufficiently large pilot gain $K^{\text{lat}}_{\varepsilon}$, the quadruple pole at the origin is stabilized by virtue of the predictor lead zeros z_1 and z_2 and one of the zeros of the PI controller z_3. The second PI controller zero is situated to the left and outside the plotting area. The plots also show that for an insufficiently large gain the system has oscillatory unstable poles. Figure 6 also shows that as T_p becomes smaller, the predictor lead zeros move away from the origin, the unstable branches extend farther in the right-half s plane, and a larger gain $K^{\text{lat}}_{\varepsilon}$ is needed to stabilize the system. Likewise, if we were to increase the constant c, the PI controller lead zero z_3 would move away from the origin, which would increase the integral action and destabilizes the system. A reasonable compromise yielding sufficient integral action and an acceptable control gain is obtained for $c = 0.96$ and $d = 5.0$, for which the PI controller zeros are at $s = -0.2$ and $s = -4.8$.

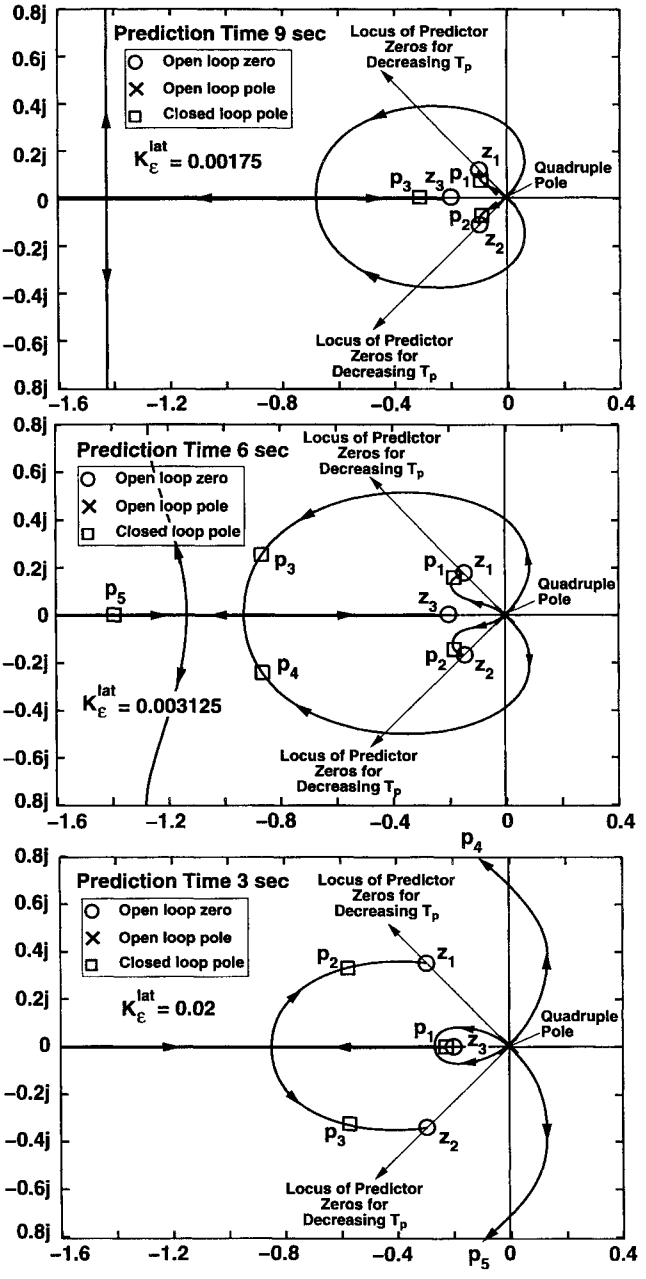

Fig. 6 Root locus plot for cutout guidance window with integral control action.

The root locus study demonstrates that for a well-chosen prediction time and pilot gain, the system can be adequately controlled by error-nulling gain control only. It is clear that besides ε_{lat}, however, the pilot has a rich set of additional cues available, e.g., bank angle and roll rate, heading angle and yaw rate, lateral deviation and deviation rate, etc. In addition, the pilot has the potential for dynamic compensation. For an incorrectly chosen prediction time, the pilot will need both to rely on these additional cues and to use dynamic compensation. For example, the large pilot gain $K^{\text{lat}}_{\varepsilon}$ required for a too small prediction time T_p might result in excessively large roll rates. The pilot, unable to realize this large gain, can no longer apply the simple proportional control law since it will result in an oscillatory unstable system, as seen in Fig. 6. Thus, additional cues like the roll rate and/or lead compensation will be required to obtain a stable loop closure. On the other hand, for a too large prediction time T_p the system might lack positional accuracy. In this case the pilot might use the positional and directional cues provided by the tunnel image, rather than the control error ε_{lat}, as loop closures.

Paper Pilot Simulations

Figure 7 shows paper pilot simulations for the described example aircraft and controller constants, for $T_p = 9$ s, for four exemplary smoothed trajectories, each of which consists of four straight and three curved sections. The paper pilot is assumed to be composed of a simple gain, i.e., the lateral control gain $K_\varepsilon^{\text{lat}}$ without the need for compensation, and a neuromuscular lag with a time constant of 0.1 s. As in Fig. 3, the curvature is expressed in terms of the equivalent bank angle ϕ, where a positive value signifies a right-hand turn. For a coordinated turn, the radius of turn for the section of constant curvature and the given velocity of $V = 220$ ft/s is $R_t = 4584$ m. The lateral control gain $K_\varepsilon^{\text{lat}}$ is set to 0.00175. Figure 7a shows the case in which no atmospheric disturbances are present. The time histories for trajectory I show that upon entering the first right-hand turn, the original predictor induces a large positive deviation of about 70 ft that indicates right corner cutting because of premature banking of the vehicle by the paper pilot. On the other hand, with the improved predictor, corner cutting is eliminated, and a slight negative deviation of about 5 ft (overshooting the curve on the left side) is noticed. Figure 7a shows that the buildup of similar errors at subsequent curvature changes is also highly reduced by the improved predictor.

Figure 7a also shows that the first right-hand turn and the subsequent left-hand turn of trajectory I allow sufficient time for the system to settle into a steady-state turn. In spite of this, the original predictor incurs a steady-state error that is caused by small biases and nonlinearities; this error is fully eliminated by the integral action of the improved predictor. Similar characteristics are noticed in the time histories for the other trajectories.

Figure 7b shows the case in which both turbulence and a steady cross wind are present. As shown in Fig. 5, turbulence p_{gust} is added to the roll rate; an rms value of 1.75 rad/s is selected for this run.

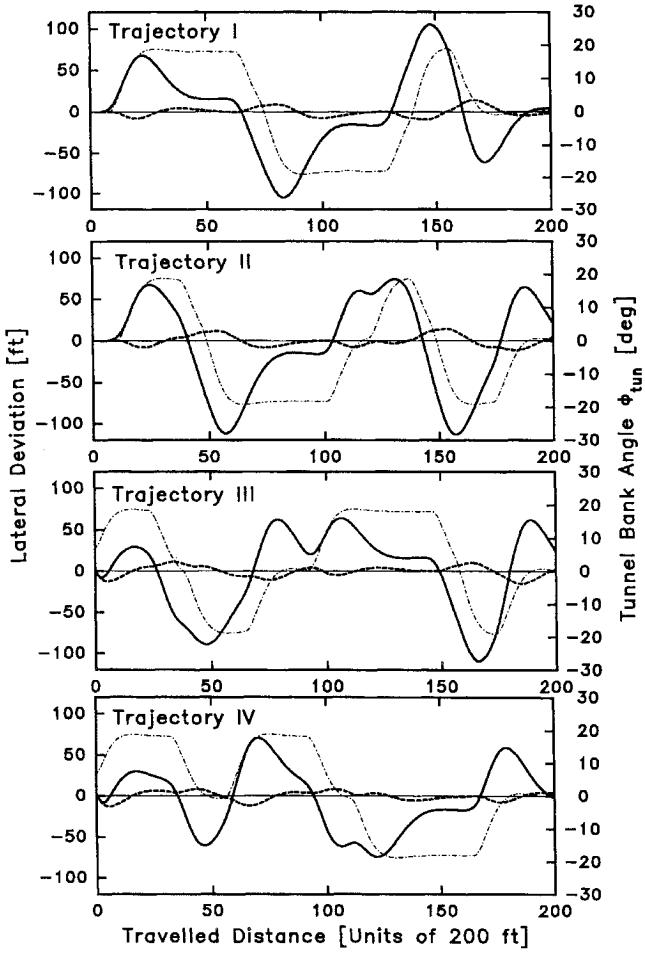

Fig. 7a Time histories of actual lateral deviation; paper pilot approach without disturbances with $T_p = 9$ s: -·-·-·-, ϕ_{tun}; ——, d_{lat} (original); - - - -, d_{lat} (improved).

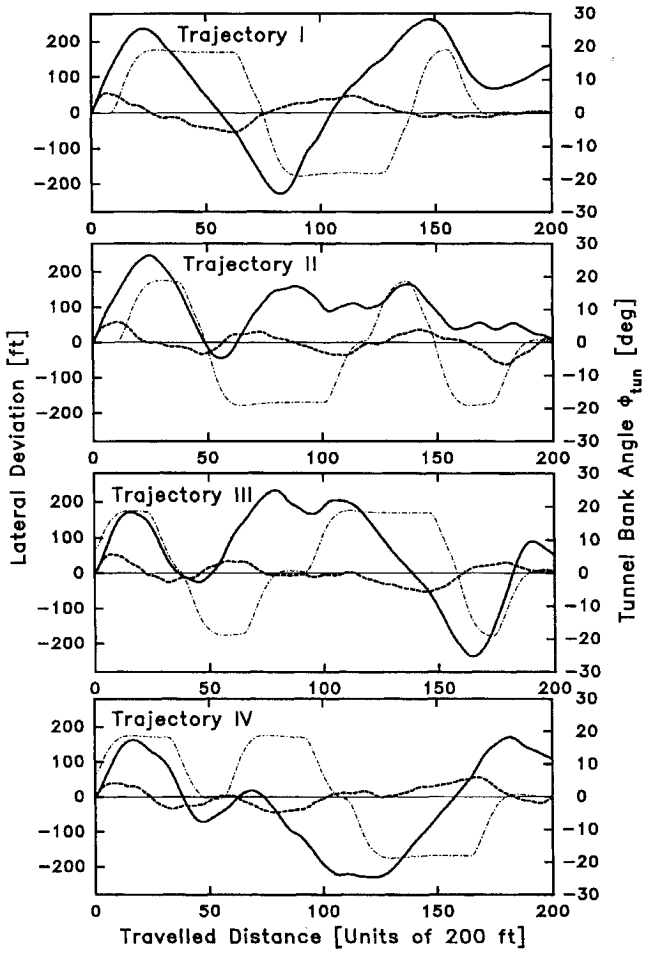

Fig. 7b Time histories of actual lateral deviation; paper pilot approach with turbulence and steady cross winds with $T_p = 9$ s: -·-·-·-, ϕ_{tun}; ——, d_{lat} (original); - - - -, d_{lat} (improved).

The steady cross winds are coming from the east, with a magnitude of 20 ft/s while the initial trajectory headings are to the north. The sideslip angle was assumed to be measured onboard with respect to the air mass rather than to a ground-based reference. As shown earlier, this will result in a steady-state error in the predicted vehicle position that is proportional to the magnitude of the cross winds. Since the vehicle heading changes along the trajectory, the magnitude of the cross winds will change accordingly, which is experienced as the slowly varying disturbance β_d appearing in Figs. 4b and 5. Figure 7b shows that the lateral deviation for the original predictor for trajectory I does not reach a steady-state value in the first right-hand turn, as in the no-disturbances case of Fig. 7a. This can be attributed to the fact that the direction of the wind relative to the aircraft changes during the turn. Figure 7b shows that the PI controller action of the improved predictor markedly reduces this deviation error. The controller parameters are chosen such that the integral action is fast enough to cope with the slowly varying disturbance during the turn. Similar characteristics are noticed for the other trajectories.

Conclusions

The improved predictor guidance scheme combines the advantage of the vehicle path predictor, being a well-designed natural flight director, conformal with the visual field, with improved bank transition behavior and improved positional accuracy in the presence of slowly varying cross winds. By providing the correct guidance information to an active cutout window, corner cutting, as experienced in large and sluggish aircraft requiring longer prediction times, is virtually eliminated. Thus, the cues derived from the relatively fast and large motions of the predictor on the screen serve in stabilizing the system by providing the necessary damping cues, and the slow and small motions of the active cutout window relative to the tunnel square

provide the integral control action that serve in reducing cross-track errors resulting from low-frequency disturbances, biases, or errors inherently present in the system.

The method of imparting guidance information to a trajectory reference, such as the tunnel cross-section, rather than including this information in the motions of the predictor is in no way restricted to reducing cross-track errors resulting from low-frequency disturbances. A challenging application would be the design of guidance information for unconventional vertical takeoff and landing aircraft, such as the Harrier or tilt rotor, that would assist the pilot in smoothly and accurately transitioning from forward to hovering flight.

The integral action tends to destabilize the system, thus increasing control activity and pilot workload. The amount of integral action that is required for reducing the effect of low-frequency disturbances on one hand and the amount that results in acceptable pilot response on the other hand might be determined by real-time pilot-in-the-loop simulator evaluations. The findings of such evaluations are presented in a companion paper.

The advantages of the circular path predictor in flying prolonged turns with zero steady-state errors, as implemented in the original tunnel display version are still present in the improved version. In a steady turn, the cutout window will be stationary with respect to the tunnel square, at a fixed displacement from its center, whereas the lateral deviation of the vehicle from the trajectory will be reduced to zero by the actions of the PI controller.

The trajectory generation algorithm appears well suited for onboard and on-site trajectory planning. It allows trajectories to be planned online, matched to the aircraft response and to its current and projected airspeed profile. En route updates of trajectory waypoints and/or airspeed can be handled by online reshaping of the trajectory.

In this study, only horizontal displacements are imparted to the cutout window since low-frequency disturbances and trajectory profiles with a constant curvature exist primarily in the horizontal plane. However, an improved vertical predictor guidance scheme can be obtained by providing the cutout window with appropriate vertical displacements as well. The development of functions for the vertical cutout window displacement is a subject of further study.

References

[1]Theunissen, E., "A Primary Flight Display for Four-Dimensional Guidance and Navigation; Influence of Tunnel Size and Level of Additional Information on Pilot Performance and Control Behavior," *AIAA Flight Simulation Technologies Conference* (Monterey, CA), AIAA, Washington, DC, 1993, pp. 140–146 (AIAA Paper 93-3570).

[2]Dorighi, N. S., Grunwald, A. J., and Ellis, S. R., "Evaluation of Perspective Displays on Pilot Spatial Awareness in Low Visibility Curved Approaches," *AIAA 8th Conference on Computing in Aerospace* (Baltimore, MD), AIAA, Washington, DC, 1991, pp. 153–157 (AIAA Paper 91-3727).

[3]Dorighi, N. S., Grunwald, A. J., and Ellis, S. R., "Perspective Format for a Primary Flight Display and Its Effect on Pilot Spatial Awareness," Digital Avionics System Conf., Seattle, WA, Oct. 1992, pp. 307–312.

[4]Dorighi, N. S., Ellis, S. R., and Grunwald, A. J., "Perspective Format for a Primary Flight Display (ADI) and Its Effect on Pilot Spatial Awareness," *Proceedings of the 37th Annual Meeting of the Human Factors and Ergonomics Society* (Seattle, WA), Human Factors and Ergonomics Society, Santa Monica, CA, 1993, pp. 88–92.

[5]Wickens, C. D., Haskell, I., and Harte, K., "Perspective Flight Displays: Application of Ergonomically Driven Display Design Principles," *Proceedings of the 1988 IEEE International Conference on Systems, Man, and Cybernetics* (Beijing and Shenyang, China), Vol. 1, Inst. of Electrical and Electronic Engineers, New York, 1988, pp. 506–509.

[6]Wickens, C. D., Haskell, I., and Harte, K., "Perspective Flight Path Displays," Aviation Research Lab., Inst. of Aviation, Final TR ARL-89-2/BOEING-89-1, Univ. of Illinois, Urbana–Champaign, IL, Feb. 1989.

[7]Reising, J., and Hartsock, D., "Pathway-in-the-Sky Evaluation," *Proceedings of the Fifth Symposium on Aviation Psychology*, Columbus, OH, 1989.

[8]Oliver, J. G., "Improving Situational Awareness Through the Use of Intuitive Pictorial Displays," Aerospace Technology Conf. and Exposition, Long Beach, CA, Society of Automotive Engineers, SAE TP 901829, Oct. 1990.

[9]Foyle, D. C., Ahumada, A. J., Larimer, J., and Townsend Sweet, B., "Enhanced/Synthetic Vision Systems: Human Factors Research and Implications for Future Systems," Enhanced Situation Awareness Technology for Retrofit and Advanced Cockpit Design, Conf. *Proceedings of the SEA Aerotech '92 Meeting* (Human Behavioral Technology/Aerospace Technologies Activity), Society of Automotive Engineers, 1992, SAE Paper SP-933.

[10]Erzberger, H., Davis, T. J., and Green, S., "Design of Center-TRACON Automation System," AGARD Guidance and Control Symposium on Machine Intelligence in Air Traffic Management, Berlin, Germany, May 1993.

[11]Grunwald, A. J., Robertson, J. B., and Hatfield, J. J., "Experimental Evaluation of a Perspective Tunnel Display for Three-Dimensional Helicopter Approaches," *Journal of Guidance and Control,* Vol. 4, No. 6, 1981, pp. 623–631.

[12]Grunwald, A. J., "Tunnel Display for Four-Dimensional Fixed-Wing Aircraft Approaches," *Journal of Guidance, Control, and Dynamics,* Vol. 7, No. 3, 1984, pp. 369–377.

[13]Grunwald, A. J., "Predictor Laws for Pictorial Flight Displays," *Journal of Guidance, Control, and Dynamics,* Vol. 8, No. 6, 1985, pp. 545–552.

[14]Blakelock, J. H., *Automatic Control of Aircraft and Missiles,* 2nd ed., Wiley-Interscience, New York, 1991, pp. 165–172.